Supporting Information

And Yet It Moves: A High-Temperature Neutron Diffraction Study of Ion Diffusion in the Inverse Perovskites $BaLiX_3$ (X = F, H, D)

Dennis Wiedemann,* Eva Maria Heppke, and Alexandra Franz

ejic201901232-sup-0001-SupMat.pdf

Table of Contents

Experimental Section

Materials: BaF_2 (Strem, 99.99%), LiF (Chempur, 99.995%), LiH (abcr, 99.4%), and LiD (Sigma-Aldrich, 98%) were bought from commercial suppliers. BaH_2 and BaD_2 were prepared in analogy to a published protocol.[1]

Syntheses: Barium lithium trifluoride, barium lithium trihydride, and barium lithium trideuteride $BaLiX_3$ (X = F, H, D) were synthesized *via* high-energy planetary ball milling in a "Fritsch PULVERISETTE 6". Equimolar amounts of the reactants LiX and BaX_2 were filled in a zirconia grinding jar (80 mL) with five zirconia grinding balls (d = 20 mm) and milled at a rotational speed of 350 rpm. On a smaller scale of typically *ca.* 3 g, a milling time of 5 h was found sufficient, whereas for *ca.* 5 g, 7 h were necessary. To enhance crystallinity, the resulting $BaLiF_3$ was annealed in a chamber furnace for 8 h at 600 °C in air. $BaLiH_3$ and $BaLiD_3$ were placed in a copper ampoule in a tube furnace and annealed for 3 h at 600 °C under a flow of Ar/H_2 (ψ = 9:1, Q = 10 L/h) or pure Ar (Q = 15 L/h), respectively.

Phase identity and purity were verified *via* powder X-ray diffraction at ambient temperature on a "PANalytical X'Pert PRO MPD" diffractometer in Bragg–Brentano (θ–θ) geometry equipped with a "PIXcel" detector using nickel-filtered Cu-K_α radiation. The number and position of reflections complied with expectations for the pure substances. No additional reflections were apparent.

Powder Neutron Diffraction: Measurements were carried out at the fine resolution powder diffractometer (FIREPOD)[2] at the *Berlin Research Reactor BER II* (HZB, Germany) with Ge(711)-monochromated neutrons (λ = 1.3084[2] Å) in Debye–Scherrer geometry. The compacted powder samples were mounted in a vacuum high-temperature furnace inside tantalum ($BaLiF_3$ at 25 °C; d = 9.7 mm, h = 55 mm) or vanadium cylinders (all other experiments; d = 5.6 mm, h = 55 mm). Measurements were carried out at room temperature and 500 °C with exposure times of *ca.* ten hours. Data were recorded with an array of eight "DENEX" ^{3}He-counter area-detectors, yielding a final range of $3° \le 2\theta \le 142°$ in steps of $\Delta(2\theta) = 0.075°$. At 700 °C, the hydrides were found to decompose rapidly—presumably into subhydrides/alloys *via* dehydrogenation—and affect the integrity of the container material.

Initial Le-Bail fits and following Rietveld refinements were carried out using JANA2006.[3] Neutron data were analytically corrected for absorption (cylindrical sample) and stripped of the irregular onset below 15° and, if necessary, of cut-off reflections above 140°. Peak profiles were fitted with a pseudo-Voigt function using the Thompson–Cox–Hastings approach (Gaussian parameters U, V, and W; Lorentzian parameter X). A zero-shift correction and a reflection asymmetry correction according to Howard were refined.[4] The background was modelled using ten Legendre polynomials interpolating between manually defined points.

As starting points for Rietveld refinements against profile data, atomic models of $BaLiX_3$ were imported from the ICSD and standardized with respect to the unit cell choice.[5] Anisotropic displacement parameters were refined for all anions, whereas cation displacement was restricted to be isotropic by site symmetry. Anharmonic terms of the fourth and sixth order for anion displacement were tested but only kept in refinement if they were significant ($|D_{ijkl}| \ge 3\sigma[D_{ijkl}]$, $|F_{ijklmn}| \ge 3\sigma[F_{ijklmn}]$) and led to a substantial drop in R values. For $BaLiH_3$ at 500 °C, this would have meant the introduction of three additional parameters per order. In this case, we refrained from our original approach because the overall very low signal-to-noise ratio (see Fig. S7) did not warrant it. Strong reflections of the tantalum container around $BaLiF_3$ at 25 °C were treated using a Le-Bail fit. Additional weak reflections conforming to a body-centered cubic lattice—possibly of a group-5 metal or iron in the beam path—were found for $BaLiF_3$ at higher and for $BaLiH_3$ at all temperatures and handled the same way. All parameters of these by-phases as well as any parameters causing correlations larger than 0.9 were fixed in the final refinement cycles.

Structure graphics were produced using Diamond 4.6 and VESTA.[6] Table S1 lists further experimental details.

MEM Reconstruction: Dysnomia 1.0 was used for maximum-entropy method (MEM) reconstruction of scattering-length densities (SLDs) from final structure factors as put out by JANA2006.[7] The unit cell was divided into $192 \times 192 \times 192$ voxels. Starting from a uniform intensity prior, the limited-memory Broyden–Fletcher–Goldfarb–Shanno (L-BFGS) algorithm[8] was employed with uncertainties augmented by E = 0.75. Relative weights, central moments, and final residuals are summarized in Table S2.

OPP Calculation: Anion one-particle potentials (OPPs) were calculated from probability-density functions (PDFs) as well as from MEM-reconstructed SLDs using CalcOPP 2.0.1.[9] In the latter case, the maximal positive (X = F, D) or negative (X = H) SLD found around the anion reference position was set to represent a potential energy of V = 0. For error estimation on PDF-derived data, the Monte-Carlo routines implemented in JANA2006 were employed (max. 10,000 iterations, final accuracy < 1%). In illustrations of SLD-derived OPPs (see Fig. 3), closed separate surfaces associated with the SLD of lithium or barium ions were cut off for the sake of clarity.

Table S1. Details of powder neutron diffractometry at λ = 1.3084(2) Å.

Empirical formula	$BaLiF_3$			$BaLiH_3$		$BaLiD_3$	
ϑ/°C	25	500	700	25	500	25	500
Container material	tantalum	vanadium	vanadium	vanadium	vanadium	vanadium	vanadium
CSD no.	1965606	1965608	1965605	1965603	1965604	1965609	1965607
Formula weight/g mol^{-1}	201.26	201.26	201.26	147.29	147.29	150.31	150.31
Crystal system	cubic	cubic	cubic	cubic	cubic	cubic	cubic
Space group	*Pm*$\bar{3}$*m* (#221)	*Pm*$\bar{3}$*m* (#221)	*Pm*$\bar{3}$*m* (#221)	*Pm*$\bar{3}$*m* (#221)	*Pm*$\bar{3}$*m* (#221)	*Pm*$\bar{3}$*m* (#221)	*Pm*$\bar{3}$*m* (#221)
a/Å	3.99348(6)	4.06276(12)	4.09432(14)	4.02593(13)	4.0959(4)	4.0135(2)	4.0849(4)
V/Å^3	63.6877(17)	67.060(6)	68.635(7)	65.253(6)	68.71(2)	64.651(10)	68.16(2)
Z	1	1	1	1	1	1	1
ρ_{calc}/g cm^{-3}	5.2479	4.9840	4.8696	3.7486	3.5597	3.8610	3.6621
μ/mm^{-1}	0.084	0.079	0.078	0.452	0.428	0.092	0.087
F(000)/fm	20.132	20.132	20.132	−8.047	−8.047	23.183	23.183
$2\theta_{max}$/°	141.789	141.789	141.789	141.789	141.789	141.789	139.991
Reflections (all, obs[a])	36, 30	38, 21	38, 22	36, 28	38, 18	36, 14	38, 13
Parameters	22	21	23	22	21	21	24
R_p, wR_p[b]	0.0255, 0.0354	0.0294, 0.0379	0.0261, 0.0335	0.0163, 0.0212	0.0176, 0.0222	0.0282, 0.0391	0.0253, 0.0336
R_{exp}, S (all)	0.0177, 2.00	0.0294, 1.29	0.0272, 1.23	0.0171, 1.24	0.0175, 1.27	0.0254, 1.54	0.0255, 1.32
R_F (obs,[a] all)	0.0242, 0.0358	0.0126, 0.0353	0.0316, 0.0495	0.0296, 0.0450	0.0578, 0.1131	0.0282, 0.0512	0.0504, 0.0935
wR_F[b] (obs,[a] all)	0.0223, 0.0250	0.0126, 0.0157	0.0279, 0.0304	0.0245, 0.0264	0.0422, 0.0519	0.0419, 0.0444	0.0428, 0.0508
R_B (obs[a])	0.0249	0.0224	0.0321	0.0484	0.0933	0.0547	0.0745
$\Delta\rho_b$(min, max)/fm Å^{-3}	−0.53, 0.82	−0.25, 0.14	−0.37, 0.31	−0.38, 0.22	−0.94, 0.62	−0.78, 0.76	−0.44, 0.35

[a] $I > 3\sigma(I)$. [b] $w = 1/[\sigma^2(I)+(0.01I)^2]$.

Diffractograms

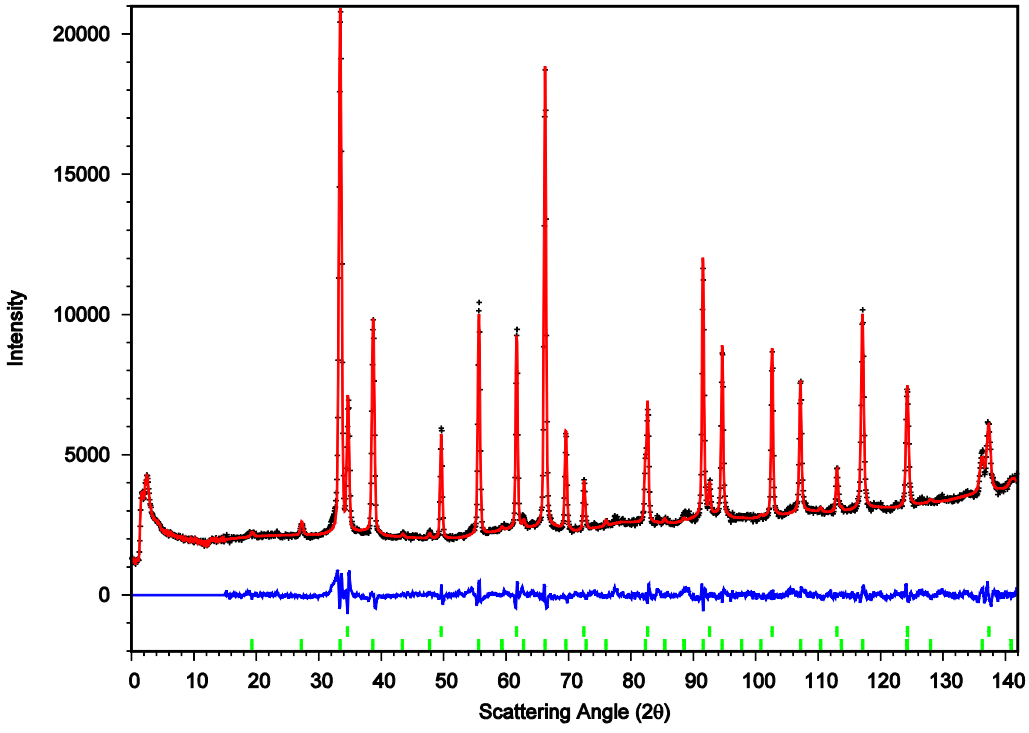

Figure S1. Neutron diffractogram of $BaLiF_3$ at 25 °C with results of Rietveld refinement. Red: calculated, black: observed, blue: difference density; green: Bragg positions for $BaLiF_3$ (bottom) and tantalum container (top).

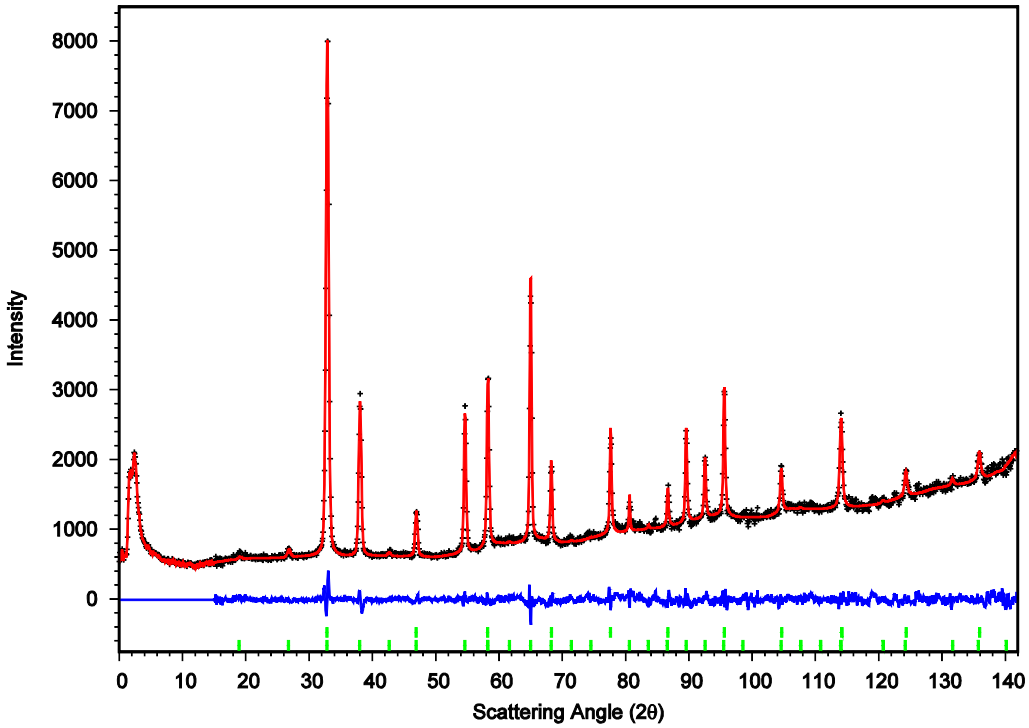

Figure S2. Neutron diffractogram of $BaLiF_3$ at 500 °C with results of Rietveld refinement. Red: calculated, black: observed, blue: difference density; green: Bragg positions for $BaLiF_3$ (bottom) and by-phase with b.c.c. lattice (top).

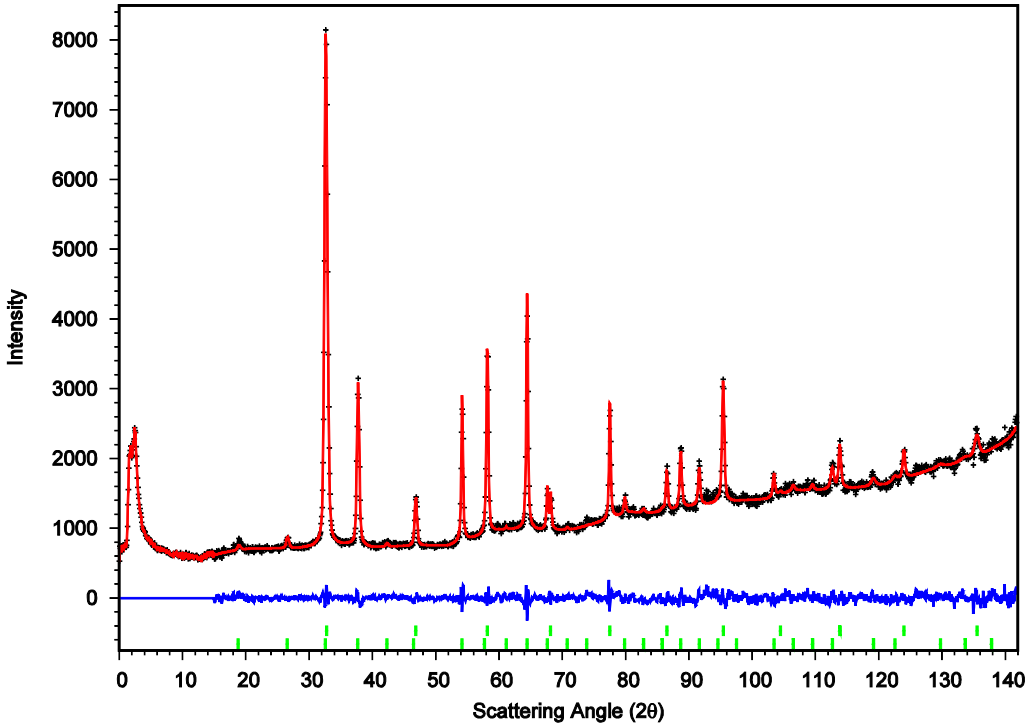

Figure S3. Neutron diffractogram of $BaLiF_3$ at 700 °C with results of Rietveld refinement. Red: calculated, black: observed, blue: difference density; green: Bragg positions for $BaLiF_3$ (bottom) and by-phase with b.c.c. lattice (top).

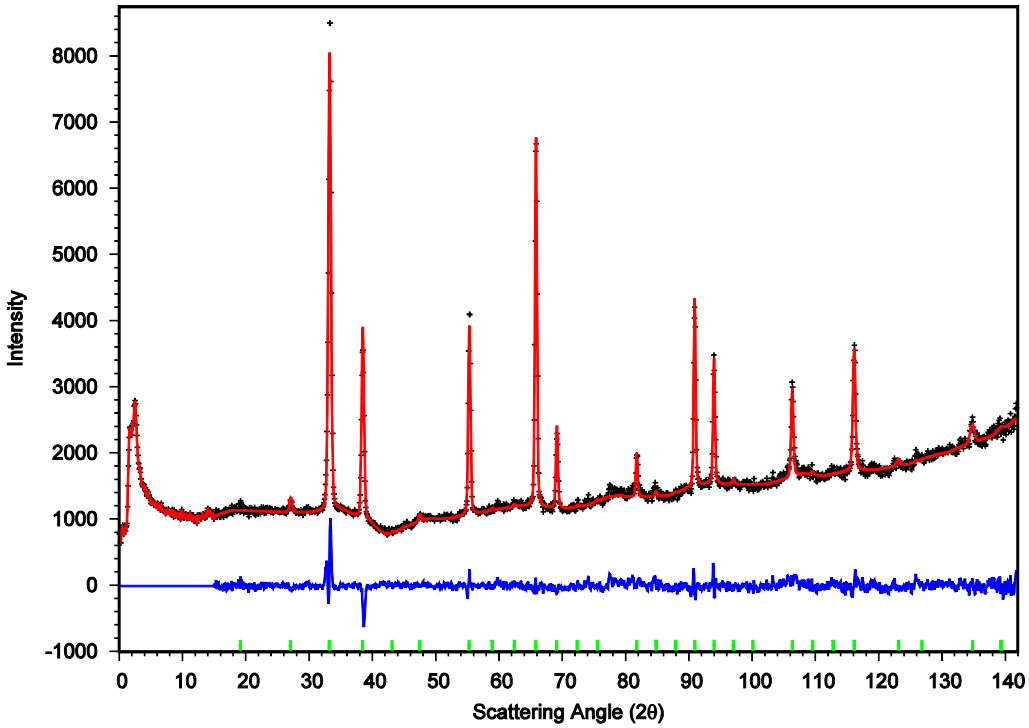

Figure S4. Neutron diffractogram of $BaLiD_3$ at 25 °C with results of Rietveld refinement. Red: calculated, black: observed, blue: difference density; green: Bragg positions. Weak additional reflections are due to impurities in the container material or the beam path.

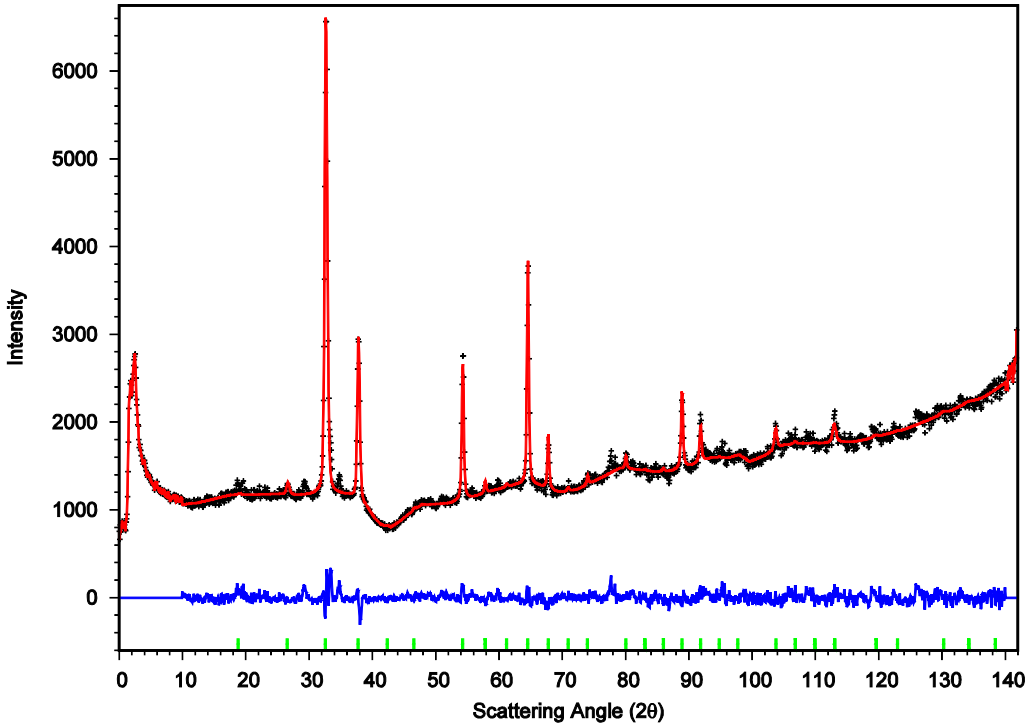

Figure S5. Neutron diffractogram of $BaLiD_3$ at 500 °C with results of Rietveld refinement. Red: calculated, black: observed, blue: difference density; green: Bragg positions. Weak additional reflections are due to impurities in the container material or the beam path.

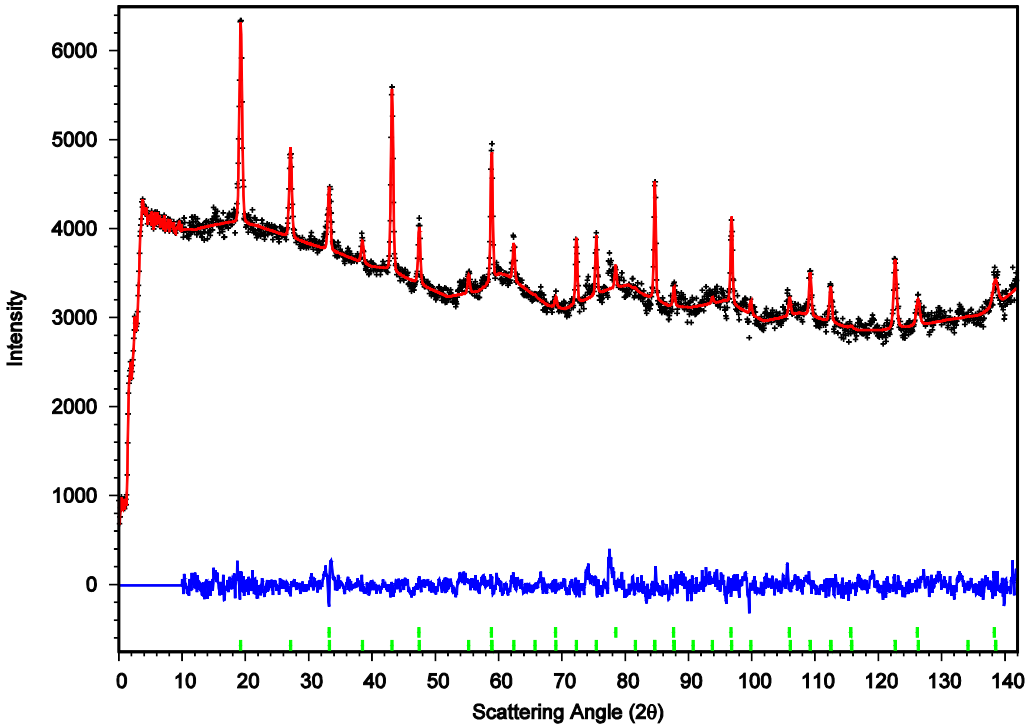

Figure S6. Neutron diffractogram of $BaLiH_3$ at 25 °C with results of Rietveld refinement. Red: calculated, black: observed, blue: difference density; green: Bragg positions for $BaLiH_3$ (bottom) and by-phase with b.c.c. lattice (top). Weak additional reflections are due to impurities in the container material or the beam path.

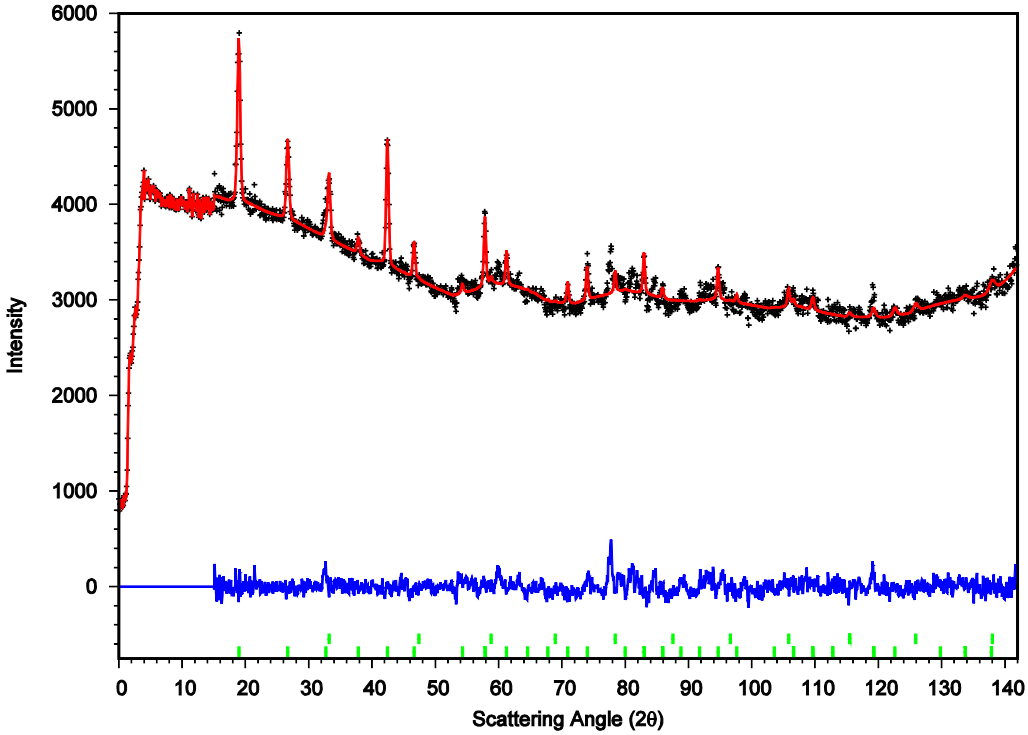

Figure S7. Neutron diffractogram of $BaLiH_3$ at 500 °C with results of Rietveld refinement. Red: calculated, black: observed, blue: difference density; green: Bragg positions for $BaLiH_3$ (bottom) and by-phase with b.c.c. lattice (top). Weak additional reflections are due to impurities in the container material or the beam path.

Crystal Structure Graphics

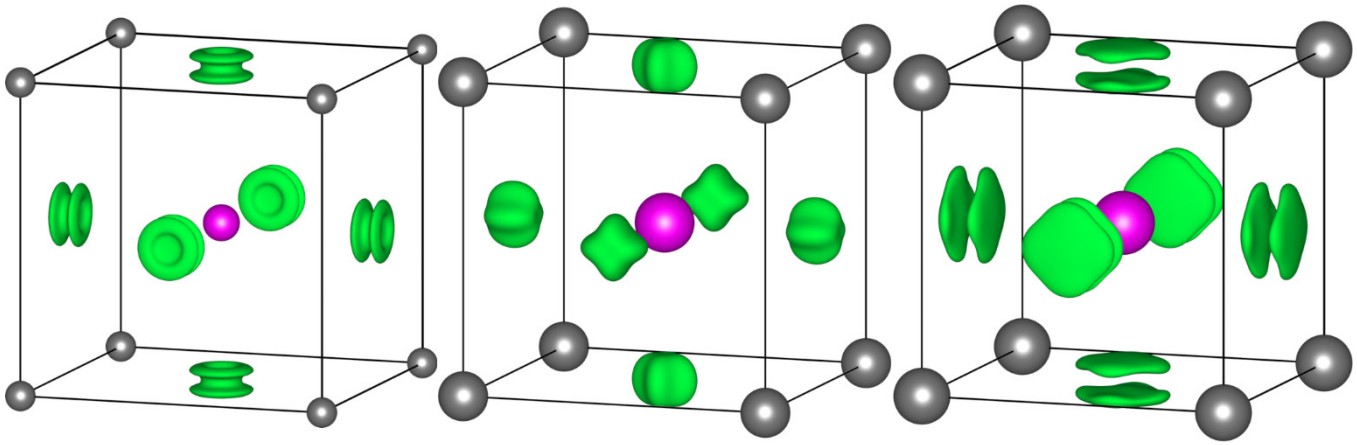

Figure S8. Crystal structure of $BaLiF_3$ at 25, 500, and 700 °C (from left to right) according to powder neutron diffraction. Barium (gray) and lithium ions (pink) as spheres of 75% probability, fluoride ions (green) as PDF isosurface of $p = 1.5$ Å^{-3}; unit cell in black.

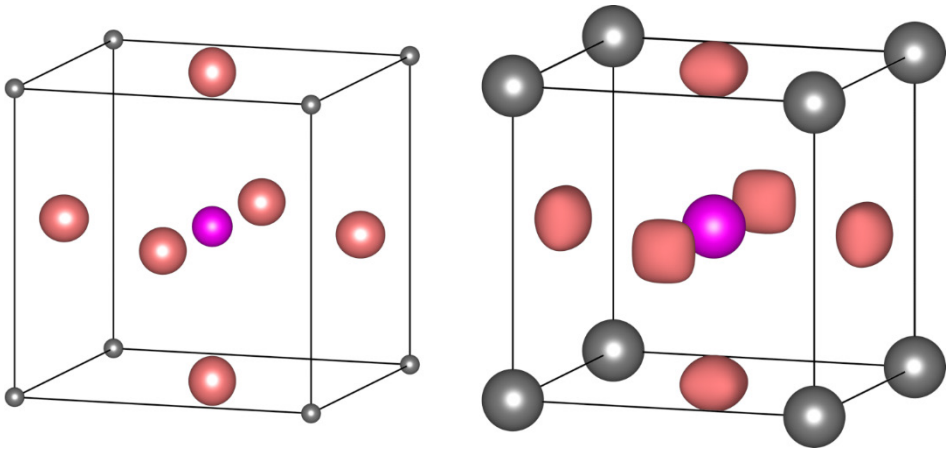

Figure S9. Crystal structure of $BaLiD_3$ at 25 (left) and 500 °C (right) according to powder neutron diffraction. Barium (gray) and lithium ions (pink) as spheres of 75% probability, deuteride ions (coral) as ellipsoids of 75% probability (left) or PDF isosurface of $p = 1.0$ Å^{-3} (right); unit cell in black.

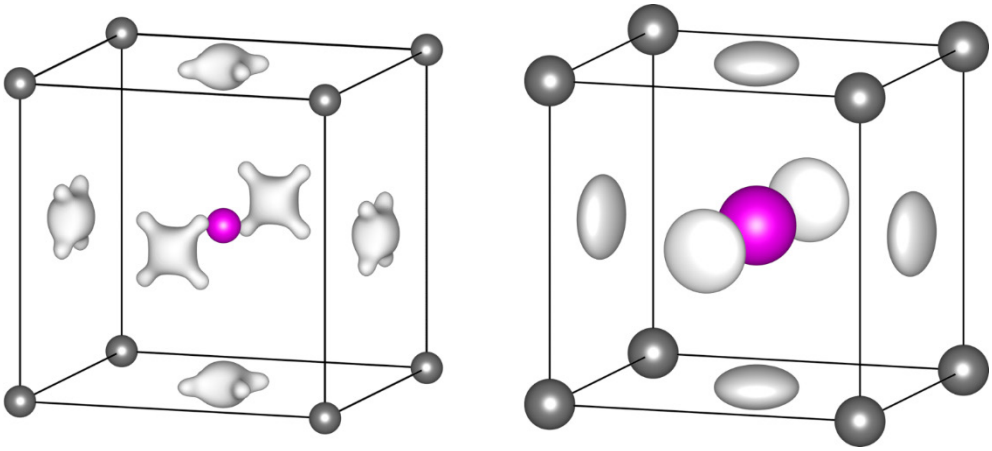

Figure S10. Crystal structure of $BaLiH_3$ at 25 (left) and 500 °C (right) according to powder neutron diffraction. Barium (gray) and lithium ions (pink) as spheres of 75% probability, hydride ions (white) as ellipsoids of 75% probability (right) or PDF isosurface of $p = 1.5$ Å^{-3} (left); unit cell in black.

Details of MEM Reconstructions

Table S2. Details of MEM reconstructions of scattering-length densities.

Formula		$BaLiF_3$	$BaLiD_3$	$BaLiH_3$
ϑ/°C		700	500	500
Relative weights of generalized constraints	λ_2	0.75	0.90	1.00
	λ_4	0.25	0.10	0
	λ_6	0	0	0
	λ_8	0	0	0
	λ_{10}	0	0	0
	λ_{12}	0	0	0
	λ_{14}	0	0	0
	λ_{16}	0	0	0
Central moments of normalized residuals	C_2	1.0001	1.0000	1.0001
	C_4	1.3267	1.3252	1.4192
	C_6	1.7980	1.8579	1.7255
	C_8	2.1498	2.2650	1.6872
	C_{10}	2.1593	2.2937	1.3576
	C_{12}	1.8242	1.9484	0.9243
	C_{14}	1.3174	1.4156	0.5447
	C_{16}	0.8278	0.8958	0.2827
R_F		0.0576	0.1006	0.1091
wR_F		0.0331	0.0414	0.0627

References

[1] N. Kunkel, H. Kohlmann, A. Sayede, M. Springborg, *Inorg. Chem.* **2011**, *50*, 5873–5875.

[2] Helmholtz-Zentrum Berlin für Materialien und Energie, *J. Large-Scale Res. Facil.* **2017**, *3*, A103; https://doi.org/110.17815/jlsrf-17813-17127.

[3] V. Petříček, M. Dušek, L. Palatinus, *Z. Kristallogr. – Cryst. Mater.* **2014**, *229*, 345–352.

[4] C. J. Howard, *J. Appl. Crystallogr.* **1982**, *15*, 615–620.

[5] G. Bergerhoff, I. D. Brown, in *Crystallographic Databases* (Eds.: F. H. Allen, G. Bergerhoff, R. Sievers), International Union of Crystallography, Chester, U.K., **1987**, pp. 77–95.

[6] a) K. Brandenburg, Diamond, Crystal and Molecular Structure Visualization, Crystal Impact – H. Putz & K. Brandenburg GbR, Bonn, Germany, **2019**; http://www.crystalimpact.com/diamond; b) K. Momma, F. Izumi, *J. Appl. Crystallogr.* **2011**, *44*, 1272–1276.

[7] K. Momma, T. Ikeda, A. A. Belik, F. Izumi, *Powder Diffr.* **2013**, *28*, 184–193.

[8] J. Nocedal, *Math. Comput.* **1980**, *35*, 773–782.

[9] D. Wiedemann, CalcOPP, Calculation of One-Particle Potentials, Technische Universität Berlin, Berlin, Germany, **2019**; https://doi.org/10.5281/zenodo.2530345.